Analysis and quantification of seabed adjacency effects in the subsurface upward radiance in shallow waters

Malik Chami, Xavier Lenot, Mireille Guillaume, Bruno Lafrance, Xavier Briottet, Audrey Minghelli, Sylvain Jay, Yannick Deville, Véronique Serfaty

Analysis and quantification of seabed adjacency effects in the subsurface upward radiance in shallow waters

MALIK CHAMI,[1,2,*] XAVIER LENOT,[3] MIREILLE GUILLAUME,[4] BRUNO LAFRANCE,[3] XAVIER BRIOTTET,[5] AUDREY MINGHELLI,[6] SYLVAIN JAY,[4] YANNICK DEVILLE,[7] AND VÉRONIQUE SERFATY[8]

[1]Sorbonne Université, CNRS-INSU, Laboratoire Atmosphères Milieux Observations Spatiales (LATMOS), boulevard de l'Observatoire, CS 34229, 06304 Nice Cedex, France
[2]Institut Universitaire de France, Ministère de l'Education Nationale, de l'Enseignement Supérieur et de la Recherche, 1 rue Descartes, 75231 Paris Cedex 05, France
[3]CS Systèmes d'Information, 5 Rue Brindejonc des Moulinais, Parc de la Grande Plaine 31506 Toulouse, France
[4]Aix Marseille Université, CNRS, Centrale Marseille, Institut Fresnel, avenue Escadrille Normandie-Niémen, 13013 Marseille, France
[5]ONERA, DOTA, The French Aerospace Lab, 2 avenue Edouard Belin, 31055 Toulouse Cedex 4, France
[6]University of Toulon, CNRS, SeaTech, Laboratoire LSIS, UMR 7296, 83041 Toulon, France
[7]Institut de Recherche en Astrophysique et Planétologie (IRAP), Observatoire Midi-Pyrénées, Université de Toulouse, UPS-CNRS-OMP, 31400 Toulouse, France
[8]DGA/DS/MRIS, 60 boulevard du Général Martial Valin, CS 21623, 75509 Paris Cedex 15, France
*malik.chami@upmc.fr

Abstract: The estimation of the bathymetry and the detection of targets located on the seabed of shallow waters using remote sensing techniques is of great interest for many environmental applications in coastal areas such as benthic habitat mapping, monitoring of seabed aquatic plants and the subsequent management of littoral zones. For that purpose, knowledge of the optical effects induced by the neighborhood of a given seabed target and by the water column itself is required to better interpret the subsurface upward radiance measured by satellite or shipborne radiometers. In this paper, the various sources of photons that contribute to the subsurface upward radiance are analyzed. In particular, the adjacency effects caused by the neighborhood of a given seabed target are quantified for three water turbidity conditions, namely clear, moderately turbid and turbid waters. Firstly, an analytical expression of the subsurface radiance is proposed in order to make explicit the radiance terms corresponding to these effects. Secondly, a sensitivity study is performed using radiative transfer modeling to determine the influence of the seabed adjacency effects on the upward signal with respect to various parameters such as the bathymetry or the bottom brightness. The results show that the highest contributions of the adjacency effects induced by the neighborhood of a seabed target to the subsurface radiance could reach 26%, 18% and 9% for clear, moderately turbid and turbid water conditions respectively. Therefore, the detection of a seabed target could be significantly biased if the seabed adjacency effects are ignored in the analysis of remote sensing measurements. Our results could be further used to improve the performance of inverse algorithms dedicated to the retrieval of bottom composition, water optical properties and/or bathymetry.

1. Introduction

The analysis of the ocean color provides pieces of information on the hydrosols, namely phytoplankton, mineral-like particles and color dissolved organic matter, and on the bottom

composition and depth when dealing with shallow waters. Such pieces of information are typically derived from the subsurface radiance that can be measured from remote sensing observations. Previous studies [1–3] proposed powerful parametric forward models to simulate shallow water radiance as a function of hydrosols, depth and bottom reflectance. Based on these models, a number of inversion algorithms have been developed to retrieve the above parameters for each pixel of a remote-sensing image [2,4–9]. These parametric models only consider one target pixel to describe the radiative transfer modeling.

Recent proximal-sensing systems, such as drones, are now able to provide high spatial resolution data. For such high spatial resolution images, adjacency effects, which represent the contamination of the radiance of a given target by photons scattered by the surrounding environment of this target, must be taken into account in order to properly derive the water composition and bottom features (e.g., depth and composition) of the target. Most of the previous studies dealing with the adjacency effects in ocean color remote sensing aimed at analyzing the influences of the atmosphere and/or of the neighboring land pixels on the radiance measured by a satellite sensor [10–20]. Here, for the first time according to our knowledge, the focus is made on the analysis of the influence of the seabed adjacency effects, which could be defined as perturbations induced by heterogeneities in the seabed reflectance on the global subsurface upward radiance in shallow waters. In particular, the contributions of the various sources of adjacency effects (i.e., water column and seabed) to the global upward radiance are quantified. The analysis of seabed adjacency effects on the subsurface radiance is important for improving the performance of inverse algorithms, such as those that rely on unmixing techniques [21]. It could also have interesting applications for the domain of underwater vision.

The objectives of this paper are (i) to propose an original analytical formulation of the subsurface upward radiance that makes explicit the terms related to the seabed adjacency effects and (ii) to analyze and quantify the seabed adjacency effects that contaminate the subsurface radiance when a given seabed target is observed. To reach these objectives, the relative importance of each oceanic radiative contribution (e.g., bottom albedo, water column) to the subsurface radiance is evaluated using radiative transfer modeling. Since the different radiative terms of the proposed analytical formulation could be computed using any radiative transfer model, the analytical formulation could thus be further used to develop inverse algorithms dedicated to the retrieval of bottom properties (depth and composition). The latter point, however, is out of the scope of the paper. The paper is organized as follows: Section 2 outlines the proposed analytical formulation of the subsurface upward radiance; Section 3 presents the results of the analysis and the quantification of the influence of seabed adjacency effects on the subsurface upward radiance. The influences of the hydrosol phase function, of the seabed target size and of the Lambertian seabed assumption are discussed in Section 4.

2. Analytical expression of the subsurface upward radiance

In this section, the analytical expression of the radiometric quantities of interest for this study are outlined, such as the subsurface upward radiance and the various terms describing the adjacency effects within the water column, based on the radiative transfer theory.

2.1. General formulation of the subsurface upward radiance

The subsurface upward radiance, hereafter referred to as L_u, depends on three main contributions [Eq. (1) and Fig. 1]:

$$L_u\left(P, 0^-, \theta_\downarrow, \theta_\uparrow, \lambda\right) = L_B^{dir}\left(P, 0^-, \theta_\downarrow, \theta_\uparrow, \lambda\right) + L_B^{dif}\left(P, 0^-, \theta_\downarrow, \theta_\uparrow, \lambda\right) + L_{udp}\left(0^-, \theta_\downarrow, \theta_\uparrow, \lambda\right) \quad (1)$$

where 0^- is the subsurface level (i.e., just beneath the air-water interface), λ is the wavelength, $\theta_\downarrow$ is the zenith angle of the solar direct downward radiance beneath the sea surface, $\theta_\uparrow$ is the zenith viewing angle of the upward radiance in the water, L_{udp} is the radiance due to photons

originating from the water column without having previously interacted with the bottom of the ocean (i.e., L_{udp} is in fact the subsurface upwelling radiance for an optically deep water), L_B^{dir} is the direct radiance which represents the photons that come directly from a seabed target pixel P up to the sea surface without being scattered by the water column, and L_B^{dif} is the radiance that represents the photons coming from all pixels located on the seabed (i.e., seabed target + neighborhood of the target) and that are scattered towards the direction of observation at the subsurface level (Fig. 1). For the sake of brevity, the dependence of the radiances with the bottom depth and with the relative azimuth angle is not introduced in Eq. (1). The dependence with the wavelength will no longer be mentioned in the following equations. For the benefit of the reader, a list of the symbols and acronyms used in the paper is provided in Appendix A.
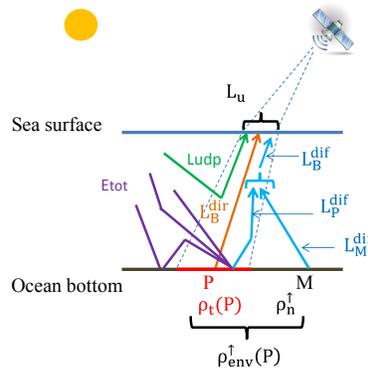

Fig. 1. Sources of the photons that contribute to the subsurface upward radiance L_u: L_{udp} is the radiance due to photons coming from the water column without having previously interacted with the bottom of the ocean, L_B^{dir} is the direct radiance that represents the photons which directly comes from a seabed target pixel P up to the sea surface without being scattered, L_P^{dif} is the diffuse radiance coming from the seabed target only, L_M^{dif} is the diffuse radiance of the neighborhood of the seabed target (excluding the seabed target), L_B^{dif} is the radiance that represents the photons coming from all pixels located in the seabed (i.e., target + neighborhood of the target M) and that are scattered towards the direction of observation at the subsurface level (L_B^{dif} is in fact the sum of L_P^{dif} and L_M^{dif}), ρ_t is the reflectance of the seabed target pixel P, $\rho_n^\uparrow$ is the reflectance of a pixel in the neighborhood of the seabed target pixel P, $\rho_{env}^\uparrow(P)$ is the reflectance caused by all the pixels located at the seabed (i.e., the seabed target P and the neighborhood of the target M), E_{tot} is the downward flux reaching the bottom.

The direct and diffuse upward radiances both depend on the incident downward flux E_{tot} that reaches the seabed. The flux E_{tot} is due to the subsurface irradiance that is directly transmitted and scattered through the water column, and also to multiple interactions between the bottom and the water column (Fig. 1). This means that the downward flux reaching the seabed target pixel is also impacted by the environment of the seabed target. Such a potential seabed adjacency effect has been evaluated and simulations revealed that neglecting the scene heterogeneity only generates less than 4% of error in the total downward flux in worst cases (not shown). Thus, the seabed adjacency effects on E_{tot} remain a secondary order term and will be neglected in the following. Such a fact is the reason for which this paper is focused on the seabed adjacency effects that affect the upward radiance (and not the downward flux).

Assuming a Lambertian bottom albedo, the direct upward radiance can be written as follows [Eq. (2)]:

$$L_B^{dir}\left(P,0^-,\theta_\downarrow,\theta_\uparrow\right) = \frac{E_{tot}(P,\ \theta_\downarrow)}{\pi} \times \rho_t\left(P\right) \times T_{dir}\left(0^-,\theta_\uparrow\right) \tag{2}$$

where ρ_t is the reflectance of the seabed target P located at the bottom level, E_{tot} is the incident downward flux at the bottom level and T_{dir} is the direct upward transmittance of the water column. Note that the use of the factor π in Eq. (2) is related to our definition of the bidirectional reflectance of the seabed target ρ_t. Such a factor π, which is homogeneous to a solid angle, is introduced to make sure that the value of ρ_t is 1 in the case of a perfect Lambertian ground reflector (i.e., flux reflected by the bottom is equal to the incident flux). Note also that the bottom upward radiance needs to be weighted by the direct upward transmittance (T_{dir}) to propagate it beneath the sea surface.

The diffuse upward radiance is obtained by integrating all radiances coming from the seabed which are scattered towards the sensor field of view as follows [Eq. (3)]:

$$L_B^{dif}\left(P,0^-,\theta_\downarrow,\theta_\uparrow\right) = T_{dif}\left(0^-,\theta_\uparrow\right)\times \iint\limits_{M\in V(P)} \frac{E_{tot}(M,\theta_\downarrow)}{\pi}\times\gamma_{env}\left(P,M\right)\times\rho_b\left(M\right)\, dS_M \quad (3)$$

where M is a pixel in the neighborhood V(P) of the seabed target P (including the target P), $\rho_b(M)$ is the reflectance of the neighboring pixel M, dS_M is the elementary surface around M, γ_{env} is the "environment weight function" that determines the contribution of a pixel M located in the neighborhood of P, and T_{dif} is the diffuse upward transmittance of the water column. Note that the use of an environmental weight function to weight the bottom albedo surrounding a target has been proposed by previous studies [18,19,22,23]. Note also that Eq. (3) implicitly assumes that the water point spread function (PSF) is parameterized here as $T_{dif} \times \gamma_{env}$. It should be highlighted that the bottom relief is not considered in this study (i.e., the bottom depths of P and M are similar). However, since our goal is to focus on the observation of the seabed at a high spatial resolution (from 0.2 to 1 m), for which the variation of the bathymetry between P and M is supposed to be weak for the majority of the bottom types found in shallow waters, the potential influence of bottom relief on the results that will be presented is likely to be weak as well. For larger spatial resolutions, it could be assumed that bottom relief might reduce the impact of seabed adjacency effects due to the increase of the distance between the target and its neighboring pixel.

Considering a uniform value of the flux E_{tot}, the diffuse upward radiance can then be written as [Eq. (4)]:

$$L_B^{dif}\left(P,0^-,\theta_\downarrow,\theta_\uparrow\right) = T_{dif}\left(0^-,\theta_\uparrow\right)\frac{E_{tot}(P,\theta_\downarrow)}{\pi}\times\rho_{env}^\uparrow\left(P\right) \quad (4)$$

where $\rho_{env}^\uparrow(P)$ is the reflectance caused by all the pixels located on the seabed that contribute to the scattered upward signal. Such a reflectance is written as follows [Eq. (5)]:

$$\rho_{env}^\uparrow = \iint\limits_{M\in V(P)} \gamma_{env}\left(P,M\right)\times\rho_b\left(M\right)\, dS_M \quad (5)$$

2.2 Analytical expression of the reflectance of the environment $\rho_{env}^\uparrow$

2.2.1 Preliminary formulation

The reflectance that is caused by the overall environment of a seabed target is obtained by integrating the bottom albedo over the area around the seabed target pixel. It is here proposed to weight the bottom albedo by a so-called "environment weight function" that is a function of the distance from the seabed target pixel.

To better distinguish the contribution of the seabed target pixel P from those of the neighboring pixels M, Eq. (5) can be re-written as follows [Eq. (6)]:

$$\rho_{env}^\uparrow\left(P\right) = \delta^\uparrow\times\rho_t\left(P\right) + \iint\limits_{M\neq P}\gamma_{env}\left(P,M\right)\times\rho_b\left(M\right)\, dS_M = \delta^\uparrow\times\rho_t\left(P\right) + \rho_n^\uparrow\left(P\right) \quad (6)$$

where $\delta^\uparrow$ is the contribution of the seabed target pixel P to the upward radiance, ρ_t is the seabed target reflectance, $\rho_n^\uparrow$ is the reflectance of neighboring pixels.

2.2.2 Expression of the environment weight function γ_{env}

As previously suggested by [18], the single scattering approximation is here used to determine the environment weight function γ_{env} (i.e., the weight that should be associated with an adjacent pixel M). Such an approximation has been used because of its convenient mathematical formulation and because Monte Carlo ray tracing (which was not available to us) would be required to properly account for the multiple scattering processes. We are aware that the single scattering approximation is one limitation of our study. However, recent results that were obtained for the case of atmospheric adjacency effects affecting ocean color remote sensing data showed that the single scattering approximation could lead to underestimate the environment radiance at short wavelengths [10]. On this basis, the results that will be presented in the current study could be examined as lower bound estimates of the influence of the seabed adjacency effects on the subsurface radiance (i.e., a higher influence might be expected if considering multiple scattering processes).

Since the photons originating from the bottom and contributing to the upward radiance are mainly concerned by the forward scattering of light by hydrosols (i.e., scattering angle ranging from 0 to 90°, Fig. 2), the anisotropy of the forward phase function of the hydrosols should be accounted for in the formulation of the environment weight function γ_{env}.
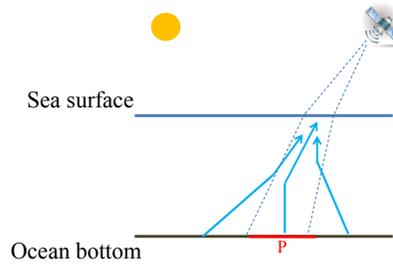

Fig. 2. Representation of the photons that contribute to the environment function γ_{env} for the diffuse upward radiance.

The environment weight function γ_{env} can be determined as follows [Eq. (7)]:

$$\gamma_{env}(M,P) = \frac{1}{S_{scene}} \times \frac{dG_{env}}{dR} \tag{7}$$

where S_{scene} is the surface of the bottom area that is considered for evaluating the effects induced by heterogeneities in the seabed reflectance on the global upward radiance, R is the distance between the center of seabed target pixel P and the center of a neighboring pixel M, and $G_{env}(R)$ is the contribution of photons originating from the surface of radius R, centered on pixel P, to the upward radiance. Actually, $G_{env}(R)$ corresponds to the weight $\delta^\uparrow$ in Eq. (6).

Assuming a uniform neighborhood of the seabed target pixel P, the function $G_{env}(R)$ could be written as follows [Eq. (8)], similarly as previously shown in [18]:

$$G_{env}(R) = \frac{\int_0^{\tau_{wtot}} \exp(-\tau_w) \int_\eta^1 \exp\left[-(\tau_{wtot} - \tau_w)/\mu\right] P(\mu) d\mu d\tau_w}{\int_0^{\tau_{wtot}} \exp(-\tau_w) \int_0^1 \exp\left[-(\tau_{wtot} - \tau_w)/\mu\right] P(\mu) d\mu d\tau_w} \tag{8}$$

where τ_{wtot} is the optical thickness of the water layer, $\eta = H/\sqrt{(H^2 + R^2)}$, H is the bottom depth, and $P(\mu)$ is the phase function of the hydrosols (μ is the cosine of the scattering angle). Note

that, as mentioned above, the formulation of $G_{env}(R)$ takes into account the anisotropy of the forward scattered radiation through the phase function.

2.3 Final formulation of the subsurface upward radiance

Based on Eqs. (1)-(6), the subsurface upward radiance that corresponds to the observation of a given seabed target P can be re-written as follows [Eq. (9)]:

$$L_u\left(P,0^-,\theta_\uparrow\right) = \frac{E_{tot}(P)}{\pi}\times\rho_t(P)\times T_{dir}\left(0^-,\theta_\uparrow\right) + \frac{E_{tot}(P)}{\pi}\times\rho_t(P)\times\delta^\uparrow\times T_{dif}\left(0^-,\theta_\uparrow\right)$$
$$+\frac{E_{tot}(P)}{\pi}\times\rho_n^\uparrow(P)\times T_{dif}\left(0^-,\theta_\uparrow\right) + L_{udp}\left(0^-,\theta_\uparrow\right) \quad (9)$$

Note that one major difference between the formulation proposed in this study [Eq. (9)] and other semi-analytical radiance models such as Lee et al.'s models [1,2] or Maritorena et al.'s model [3] relies on the explicit occurrence of the term that represents the adjacency effects induced by the neighboring pixels, $\rho_n^\uparrow(P)$.

3. Estimation of the influence of adjacency effects on the subsurface upward radiance

In this section, the influence of the adjacency effects induced by heterogeneities in the seabed reflectance and by the water column itself on the global subsurface radiance is investigated based on theoretical background (Section 2) and on radiative transfer modeling. The OSOAA radiative transfer model [24] is used to carry out simulations for that purpose. The OSOAA model is able to simulate the flux and the radiance for any observation geometry at any depth within the water column using the optical properties of the hydrosols (e.g., absorption, scattering and backscattering coefficients) as inputs. Different types of hydrosols such as phytoplankton-like particles (characterized by the chlorophyll *a* concentration), mineral-like particles (hereafter denoted as "SED"), and colored dissolved organic matter (hereafter denoted CDOM) could be used in the OSOAA model. The reader is referred to Chami et al. [24] for more details concerning the description of the OSOAA model.

3.1 Estimation of the environment function $G_{env}(R)$

The function $G_{env}(R)$ has been calculated using Eq. (8). The OSOAA model has been used to compute the radiative terms that are involved (e.g., phase function of the hydrosols, transmission, radiance of the seawater). The computations are carried out for three water types, namely clear water, moderately turbid water and turbid water. The inputs of the simulations are reported in Table 1. The phase functions of hydrosols are obtained from Mie theory using a refractive index value of 1.05 for phytoplankton-like particles, of 1.20 for mineral-like particles and a Junge size distribution of exponent 4. Mie theory was used because the polarized phase function of hydrosols is required to correctly simulate the unpolarized radiance.

Table 1. Parameters used as inputs in the OSOAA model: a_{CDOM} (440 nm) is the absorption coefficient of CDOM at 440 nm, the CHL concentration is in mg m^{-3}, the SED concentration is in mg L^{-1}, τ_w is the water optical depth at 550 nm.

Wavelength (nm)	443, 490, 510, 550, 660		
Solar zenith angle θ_s	30°		
Zenith viewing angle θ_v	30°		
Relative azimuth	180° (i.e., specular plane)		
Bottom depth H (m)	1 ; 5 ; 10		
Water turbidity	CHL (mg m^{-3})	SED (mg L^{-1})	a_{CDOM} (440 nm) (m^{-1})
Clear water	0.03	0	0

Moderately turbid water	1	3	0.2
Turbid water	30	30	1
	τ_w(550 nm, H = 1 m)	τ_w(550 nm, H = 5 m)	
Clear water	0.09	0.47	
Moderately turbid water	0.94	4.71	
Turbid water	8.01	30.0	

Figure 3 shows the results of the computations of G_{env} for bottom depth values of 1 m and 5 m. Since the results are quite similar for the three water turbidities, only the results regarding the moderately turbid water are shown.
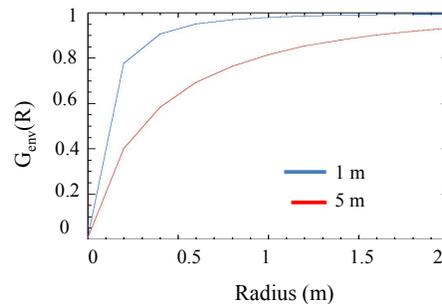

Fig. 3. Environment function $G_{env}(R)$ (or $\delta^\uparrow$) [Eq. (8)] at 550 nm, as a function of the radius R of a circular target P for bottom depth values of 1 m and 5 m and for the moderately turbid water condition.

The function $G_{env}(R)$ significantly depends on the size of the seabed target and on the bathymetry. In particular, the radiative contribution G_{env} of the seabed target pixel P to the diffuse upward radiance strongly depends on the target size when the radius of the seabed target is lower than 0.5 m where a sharp increase is observed at a bottom depth of 1 m (Fig. 3). When the seabed target size is sufficiently large (i.e., radius values R greater than 1 m) and for very shallow waters (bottom depth of 1 m), the photons contributing to the upward radiance mainly originate from the seabed target itself (i.e., G_{env} is close to 1), which means that the influence of neighboring pixels could thus be neglected for these shallow water conditions. Conversely, the influence of neighboring pixels could not be neglected for small seabed targets and/or deep waters. It is interesting to note that a similar sharp increase of G_{env} at low radius has been observed for environmental effects induced by atmospheric scattering [18].

3.2 Quantification of the adjacency effects due to seabed heterogeneities and the water column

In this section, the overall adjacency effects induced by heterogeneities in the seabed reflectance and by the water column itself on the global upward subsurface radiance are quantified. For that purpose, the bottom albedo is modeled for two configurations (Fig. 4): (i) a bright seabed target of reflectance ρ_c surrounded by dark pixels having a bottom albedo ρ_d (case 1), (ii) a dark seabed target of bottom albedo ρ_d surrounded by bright pixels of bottom albedo ρ_c (case 2). Such configurations are used to get a maximum of contrast between the target and its neighborhood.

The bottom reflectances of dark and bright pixels are taken from a library of reflectance spectra that can be encountered in natural waters (Table 2) [25]. To evaluate the highest theoretical impact of bottom heterogeneities on the subsurface radiance, the maximum contrast is practically obtained by selecting the highest and lowest bottom albedo values within our available database for a given wavelength.
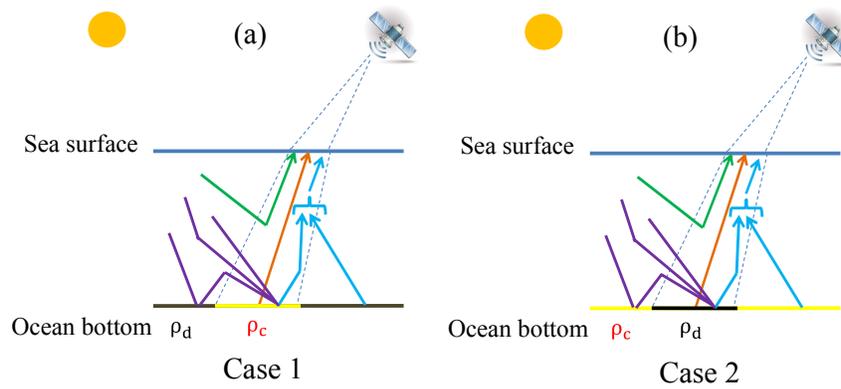
Fig. 4. Representation of the two configurations that are used to model the bottom albedo: (a) a bright seabed target of reflectance ρ_c surrounded by dark pixels having a low bottom albedo ρ_d (case 1), (b) a dark seabed target of bottom albedo ρ_d surrounded by bright pixels having an albedo ρ_c (case 2).

Table 2. Bottom albedo values that are used for bright and dark pixels as inputs of the radiative transfer modeling at various wavelengths.

Wavelength	443 nm	490 nm	510 nm	550 nm	660 nm
Bottom albedo of bright pixel ρ_c	0.16	0.16	0.16	0.23	0.23
Bottom albedo of dark pixel ρ_d	0.01	0.01	0.01	0.03	0.02

The analytical formulation of the subsurface upward radiance [Eqs. (1) and (9)] is useful to express the contributions of both seabed heterogeneities (represented by the term L_B^{dif} in Fig. 1) and the scattering events induced by the water column itself (represented by the term L_{udp} in Fig. 1). A sensitivity study is now performed to quantify these contributions (L_B^{dif} and L_{udp}) on the subsurface upward radiance.

3.2.1 Quantification of the importance of seabed contributions at the subsurface level

To quantify the importance of the sole seabed background at the subsurface level, a specific case is added in the radiative transfer simulations; such a specific case consists in removing the influence of the neighboring pixels on the upward radiance so that only the contribution of the seabed target P to the upward radiance exists. Such a case is easily obtained by setting the value of the coefficient $\delta^\uparrow$ to one in Eq. (6) and in the simulations (i.e., the weight of the neighboring pixels is zero). The relative variation of seabed contributions at the subsurface level when accounting for or neglecting seabed heterogeneities is then calculated through the relative difference ratio Δ [Eq. (10)]:

$$\Delta = \frac{\left| [L_B^{dir} + L_B^{dif}](\delta^\uparrow) - [L_B^{dir} + L_B^{dif}](\delta^\uparrow = 1) \right|}{[L_B^{dir} + L_B^{dif}](\delta^\uparrow)} \tag{10}$$

Actually, Δ is calculated using the terms that accounts for the bottom influence only, namely, L_B^{dir} and L_B^{dif}, and not the term contributing to the water column (L_{udp}). The terms that are required for estimating the subsurface upward radiance using the analytical expression [Eq. (9)], such as the downward flux E_{tot}, the transmittances T_{dir}, T_{dif}, and the contribution of the seabed target $\delta^\uparrow$, were computed using OSOAA model for the two bottom configurations as represented in Fig. 4 (case 1 and case 2). The influence of various parameters, namely the bottom depth (1 m, 5 m, 10 m) and the water turbidity (clear, moderately turbid, turbid), on the relative variation is also investigated. The results are presented for a seabed target radius value of 0.2 m (Fig. 5).

Figure 5 shows that the relative influence of the seabed adjacency effects is often much higher in the configuration of a bright neighborhood/dark seabed target (case 2) than in the opposite configuration (i.e., dark neighborhood/bright seabed target), which is expected as a result of the brightness of the neighboring pixels. As an example, the relative variation Δ is six times greater for case 2 than case 1 for clear water conditions at 450 nm when the bottom depth is 5 m; the relative variation Δ is 10% and 60% for cases 1 and 2 respectively. Note that the relative variation shown in Fig. 5 quantify the highest variation of the seabed contributions since the two configurations that are studied here approximately represent the optimum contrast that could be found in natural waters.

Figure 5 also shows that the seabed contributions significantly depend on the bathymetry. The relative variation Δ typically decreases for shallower waters from 5 m to 1 m. As an example, Δ decreases by a factor of 6 for such bathymetry range at 450 nm for clear water conditions in case 2. It means that the seabed target is the main contributor to the upward photons having interacted with the bottom at low bathymetry (e.g., 1 m) and the influence of neighboring pixels is significantly reduced for such shallow waters. This is because there is less likelihood of photons originating from neighboring pixels being re-oriented toward the radiometer in the case of a thin oceanic layer. Conversely, photons originating from the neighboring pixels are more likely to be propagated toward the sensor for deeper waters.

The maximum relative variation Δ is often observed at short wavelengths (440 nm) whatever the water turbidity. The maximum value of Δ reaches about 60% for the clear water case when the bottom depth value is 5 m, 120% for the moderately turbid water case when the bottom depth value is 5 m, and about 55% for the turbid water case when the bottom depth value is 10 m. Note that Δ value could be greater than 100% for some specific conditions in the case 1 configuration. It could be explained as follows. Since the seabed target is brighter than the neighboring pixels for such a case 1, the value of the term $[L_B{}^{dir} + L_B{}^{dif}](\delta^{\uparrow} = 1)$ is systematically greater than $[L_B{}^{dir} + L_B{}^{dif}](\delta^{\uparrow})$. For a given depth, $[L_B{}^{dir} + L_B{}^{dif}](\delta^{\uparrow})$ value could decrease (i.e., weaker influence of the neighboring pixels) while the value of the term $[L_B{}^{dir} + L_B{}^{dif}](\delta^{\uparrow} = 1)$ could be greater by more than 2 times than the $[L_B{}^{dir} + L_B{}^{dif}](\delta^{\uparrow})$ value, thus resulting in a value of Δ greater than 100%. Such a specific condition happens for the moderately turbid water configuration at 5 m [Fig. 5(b)]. Conversely, since the seabed target is always darker than the neighboring pixels in the case 2 configuration, the $[L_B{}^{dir} + L_B{}^{dif}](\delta^{\uparrow})$ value is systematically greater than that of $[L_B{}^{dir} + L_B{}^{dif}](\delta^{\uparrow} = 1)$, thus resulting in a value of Δ remaining always lower than 100%. The mean relative variation on seabed contribution, Δ_{mean}, has been calculated over the five wavelengths and over the two bottom configurations (cases 1 and 2). Δ_{mean} is reported in Table 3.
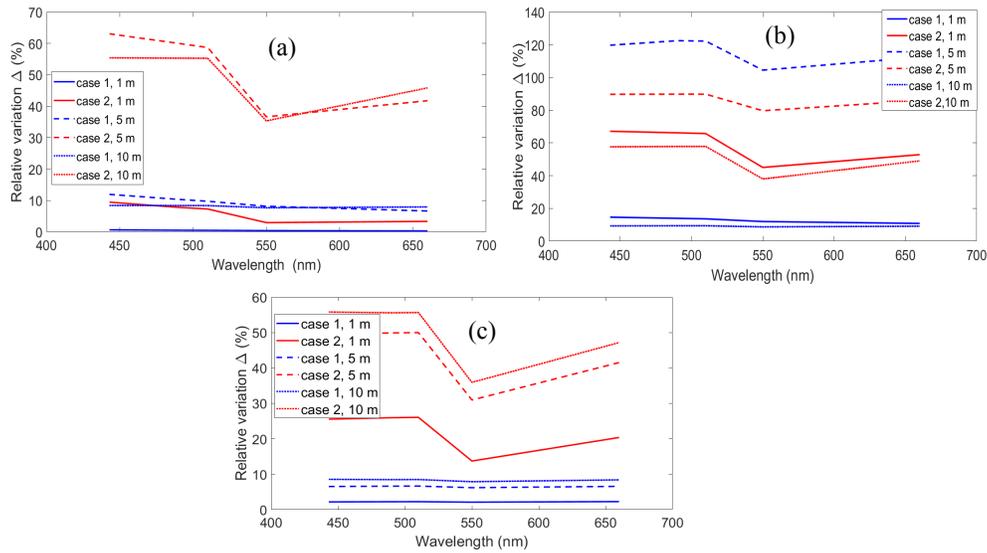
Fig. 5. Relative variation of seabed contributions Δ (in %) at the subsurface level when accounting for or neglecting seabed heterogeneities (i.e., the weight of the seabed target is maximum when heterogeneities are neglected; $\delta^\uparrow = 1$) for three water turbidity conditions (a) clear water, (b) moderately turbid water, (c) turbid water. The results are presented for the following conditions: target size radius of 0.2 m, three bottom depth values (1 m, 5 m, 10 m) and two bottom albedo configurations (bright and dark seabed target/neighboring pixels as illustrated in Fig. 4).

As observed in Fig. 5, Table 3 shows that the mean relative variation Δ_{mean} highly decreases for shallower waters from 5 m to 1 m. Table 3 also indicates that the mean relative variation is higher for the moderately turbid water case than for the clear and turbid water conditions. Such variations of Δ_{mean} with the water turbidity could be explained as follows. For clear water conditions, the contribution of the direct light component from the bottom to the sea surface dominates relatively to the other components of the radiance, thus reducing the relative seabed contribution from the neighboring pixels. For the turbid water conditions, the bottom of the ocean can hardly be viewed from the sea surface, which also reduces the influence of the seabed adjacency effects.

Table 3. Mean value of the relative variation of seabed contributions Δ_{mean} (in %); the seabed target size radius R value is 0.2 m; the bottom depth values are 1, 5 and 10 m for three water turbidity conditions (clear, moderately turbid and turbid waters). σ is the standard deviation (in %).

Bottom depth (m)	Clear water	Moderately turbid water	Turbid water
1	3 (σ = 4)	36 (σ = 25)	12 (σ = 11)
5	30 (σ = 24)	102 (σ = 16)	25 (σ = 21)
10	29 (σ = 23)	31 (σ = 23)	29 (σ = 22)

3.2.2 Quantification of the overall adjacency effects (seabed heterogeneities and water column) on the subsurface upward radiance

The OSOAA radiative transfer model is used to simulate all the terms that contribute to the subsurface upward radiance [Eq. (1)], namely L_B^{dir}, L_B^{dif}, L_{udp}, for the three water turbidities, for a pixel size radius value of 0.2 m and a bottom depth value of 5 m. Note that it is also the first time, to our knowledge, that the relative importance of the effects induced by the light scattered by the water column itself (i.e., term L_{udp} in [Eq. (9)]) on the subsurface upward radiance is studied. A biogenic seabed target, which is composed of 50% of *Posidonia* species and of 50% of *Caulerpa Taxifolia* species, is used. The neighboring pixels are composed of sand (i.e., bright environment). Note that such a configuration of bottom composition is

frequently observed in the Mediterranean Sea [26], and is thus consistent with bottom albedo reflectance spectra found for real-world conditions. Figure 6(a) shows the bottom reflectance spectra of the biogenic seabed target and of the neighboring pixels. It is observed that the bottom albedo of the target shows a maximum value around 550 nm in the visible spectrum and a sharp increase of the reflectance in the near infrared starting at 700 nm, as expected from the typical optical properties of vegetation-like hydrosols. The sand reflectance continuously increases from 400 nm to 700 nm, with values higher than the seabed target reflectance.

The two terms that compose the environment reflectance [Eq. (6)], namely $\delta^{\uparrow} \times \rho_t$ and $\rho_n^{\uparrow}$, are represented in Figs. 6(b)-6(d) for the clear water condition and for various bottom depth values. Those Figs. clearly show the increasing relative influence of the sand pixels upon the seabed target reflectance when the bathymetry increases. As an example, the ratio between the seabed target reflectance (red line) at 550 nm and the neighbor environment reflectance (blue line) at 550 nm is about 2 at 5 m [Fig. 6(b)] compared to 1 at 10 m [Fig. 6(c)] and 0.5 at 15 m [Fig. 6(d)]. As mentioned above, photons coming from neighboring pixels are more likely to be received by a subsurface sensor for deeper waters, thus increasing the potential contribution of the neighboring environment relatively to the observed seabed target.

The various radiance contributions to the subsurface upward radiance, namely the terms L_B^{dir}, L_B^{dif}, L_P^{dif}, L_M^{dif} and L_{udp} (Fig. 1), are plotted in Figs. 7(a)-7(c) for the three water turbidity conditions and for a bottom depth value of 5 m.

In the clear water condition, the major contribution to the subsurface upward radiance is the direct radiance L_B^{dir} [Fig. 7(a)], as expected since the quantity of hydrosols in the water column is very low. As a result, the radiance shows a maximum at 550 nm, similarly as the bottom albedo. The contribution of the diffuse radiance originating from the seabed target (L_P^{dif}) is also significant in the green although it is much lower in magnitude (by a factor of 7) than the contribution of L_B^{dir}. Note that the contribution of the photons scattered by the water column itself without having interacted with the bottom (L_{udp}) is not negligible in the blue part of the spectrum (at 400 nm) relatively to the direct light; this is because of the scattering of light by water molecules. The contribution of L_{udp} thus decreases at higher wavelengths.
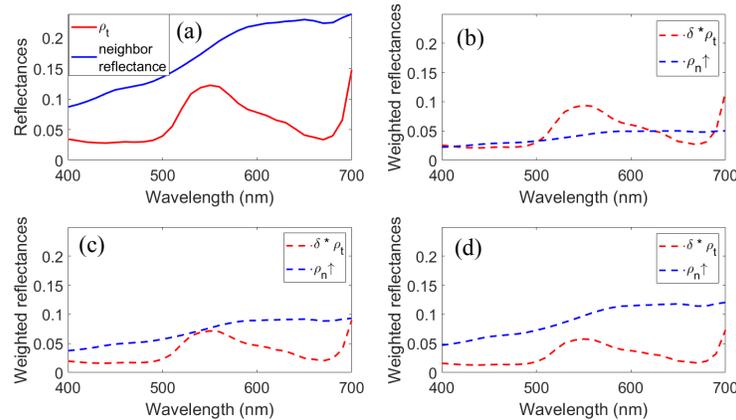

Fig. 6. (a) Bottom reflectance spectra ρ_t of the seabed target (mix of the biogenic species *Posidonia* and *Caulerpa Taxifolia*) (red line) and its neighboring pixels (sand, blue line) ; Figs. 6(b)-6(d) show the terms $\delta^{\uparrow} \times \rho_t$ (red dotted line) and $\rho_n^{\uparrow}$ (blue dotted line) of the environment reflectance [Eq. (6)] for the clear water condition and for various bottom depth values: (b) 5 m, (c) 10 m, (d) 15 m.

In the moderately turbid water condition, both components related to the diffuse radiance L_P^{dif} and to the radiance L_{udp} are the major contributors to the subsurface radiance [Fig. 7(b)]; their magnitude is fairly similar at 550 nm. However, the spectral shapes of the radiances

differ; the diffuse radiance L_P^{dif} shows a bell spectral shape with a narrow peak centered at 550 nm while the spectral variation of the radiance L_{udp} and L_M^{dif} show wider peaks over the visible spectrum, especially for L_{udp}. The narrow peak observed for L_P^{dif} is expected due to the spectral signature of the seabed target [Fig. 6(a)]. The spectral shape of L_{udp} is consistent with both the spectral variation of the scattering by water molecules, which is higher in the blue domain, and the spectral variation of the scattering by hydrosols (phytoplankton and mineral-like particles), which is significant in the blue/yellow part of the spectrum. The contribution of the radiance induced by the bottom albedo (L_M^{dif}) is about half lower at 550 nm than that of L_{udp} while the contribution of the direct radiance (L_B^{dir}) is about 5 times lower than that of L_{udp}.

In the turbid water condition, the subsurface upward radiance is almost only induced by the photons scattered by the water column itself without having being subjected to any interaction with the bottom (i.e., L_{udp}) [Fig. 7(c)]. The contribution of the neighboring pixels to the subsurface radiance, which is more than one order of magnitude lower than L_{udp}, is thus negligible here. Such a high contribution of L_{udp} is foreseeable since the number of scattering events induced by the hydrosols drastically increases in such turbid conditions, thus masking the influence of the bottom on the radiation at the sea surface.

The ratio $\Delta AE = [L_B^{dif}(\delta)-L_B^{dif}(\delta = 1)]/L_u$ is informative on the seabed adjacency effects on the subsurface upward radiance since it represents the relative difference in the total subsurface radiance when accounting for or neglecting seabed heterogeneities. Such a ratio is plotted in Figs. 7(d)-7(f) to quantify the influence of these adjacency effects. The magnitude of the seabed adjacency effects induced by the neighboring pixels is the lowest for turbid waters (the maximum value of ΔAE is 0.014 at 550 nm) relative to the clear and moderately turbid conditions [Figs. 7(d)-7(f)]. This is consistent with the fact that the scattering events induced by hydrosols, and thus the water column itself, are the major process contributing to the radiance. The highest value of ΔAE is observed for moderately turbid waters where the values are higher by one order of magnitude than in the turbid case (0.16 compared to 0.014) and by a factor of 3 (0.2 compared to 0.06) than in the clear water case at 550 nm. The ratio shows lower values in the clear water case [Fig. 7(d)] than in the moderately turbid case [Fig. 7(e)] because the scattering of light by hydrosols is not sufficiently pronounced to propagate the bottom radiance up to the subsurface. Note that the minimum value of the ratio observed at 550 nm for the clear and moderately turbid water conditions is explained by the bottom albedo of the aquatic plants, which reaches its maximum at such wavelengths and thus, the contribution of the direct light increases as mentioned above.

The maximum values of the spectral ratio ΔAE for each water turbidity condition and for various bathymetries, namely 1 m, 2 m, 3 m, 4 m, 5 m, 10 m, 15 m are reported in Table 4.
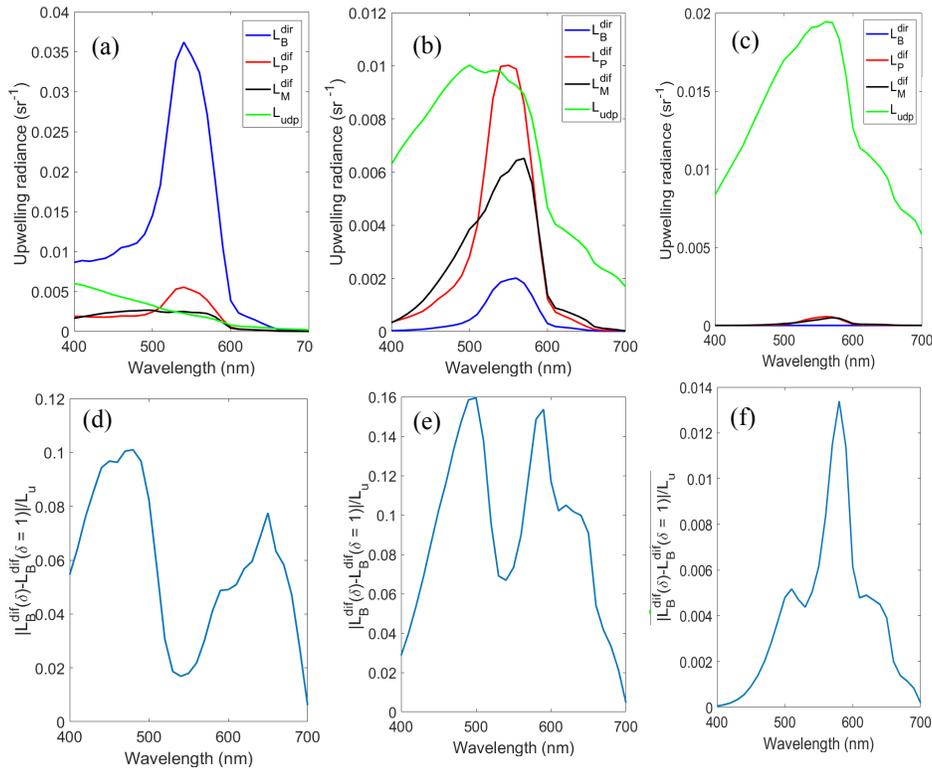
Fig. 7. Representation of the various radiances that contribute to the subsurface upward radiance, namely L_B^{dir}, L_P^{dif}, L_M^{dif} and L_{udp}, for (a) clear water, (b) moderately turbid water and (c) turbid water. Representation of the ratio $\Delta AE = [L_B^{dif}(\delta)-L_B^{dif}(\delta = 1)]/L_u$, which quantifies the seabed adjacency effect, for (d) clear water, (e) moderately turbid water and (f) turbid water. The bottom depth value is 5 m.

Table 4. Maximum values of the spectral ratio ΔAE for various bottom depths and for various water turbidity conditions.

	1 m	2 m	3 m	4 m	5 m	10 m	15 m
Clear water	0.006	0.02	0.05	0.07	0.10	0.21	0.26
Moderately turbid water	0.06	0.15	0.18	0.17	0.16	0.07	0.02
Turbid water	0.08	0.09	0.05	0.03	0.01	0.00	0.00

Table 4 points out that the bathymetry and the turbidity both play an important role in the seabed adjacency effects on the subsurface upward radiance. The clear water case shows that the contribution of the seabed adjacency effects regularly increases with the bottom depth up to 15 m to reach 26% (i.e., 0.26); the moderately turbid case shows that the contribution of seabed adjacency effects reaches its maximum (18%) for a bottom depth value of 3 m, while the maximum value is reached for a bottom depth of 2 m in the turbid water case (9%). The shift of the maximum value of the contribution of seabed adjacency effects toward lower depths when the turbidity increases suggests that the magnitude of the seabed adjacency effects is somehow weighted by each of these two parameters in a complex manner. For the clear water condition, ΔAE increases with depth partly because the value of L_u decreases due to the decreasing influence of the direct radiance L_B^{dir}. For the turbid water condition, the contribution of L_{udp} is so strong that it could mask the bottom for high bottom depth values (e.g., 15 m); as a result, the term L_M^{dif} is negligible relatively to L_{udp} thus leading to a weak value of the term $L_B^{dif}(\delta)$. Note, however, that the contribution from the bottom, L_M^{dif}, could be sufficiently high for low bottom depth values (e.g., 2 m) to make ΔAE value greater. The

maximum values of ΔAE that is observed for moderately turbid water between 3 and 5 m seem to be a balance between the moderate decrease of L_u on the one hand and the moderate increase of L_M^{dif} on the other hand.

Figure 8 shows the various contributions of the adjacency effects to the subsurface upward radiance for a bottom depth of 15 m in the clear water case only.
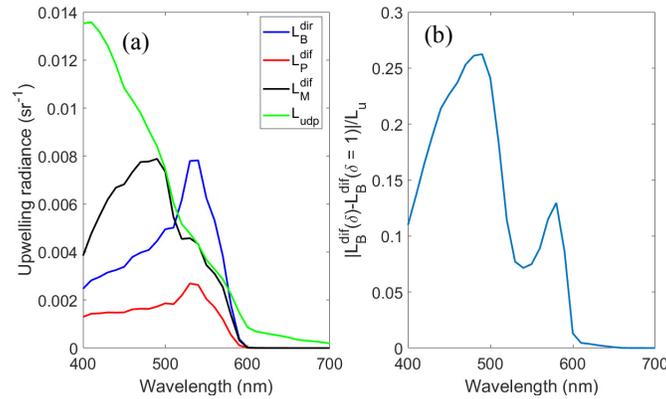

Fig. 8. Same as Fig. 7 but for a bottom depth value of 15 m and for the clear water case: (a) representation of the various radiances that contribute to the subsurface upward radiance, (b) ratio ΔAE.

It is observed that the influence of the adjacency effects induced by seabed heterogeneities is greater by almost a factor of 2.5 at 15 m (26% at 480 nm, [Fig. 8(b)]) than that found when the bottom depth is 5 m (10% at 480 nm) [Fig. 7(d)], because the relative contribution of the direct light decreases from 15 m to 5 m [Fig. 7(a) and Fig. 8(a)].

The results presented in Fig. 7, Fig. 8 and Table 4 show that the influence of seabed adjacency effects induced by seabed heterogeneities and by the scattering events within the water column itself could significantly depend on the bottom depth and the turbidity of the water column. Typically, the radiance that is ascribed to these effects could contribute up to 26% and 18% to the subsurface radiance for clear and moderately turbid waters, respectively. Therefore, the adjacency effects should not be neglected when observing a seabed target at a high spatial resolution using remotely-sensed data. However, when the turbidity of the water significantly increases, the seabed adjacency effects on the subsurface radiance are masked because of the greater influence of the water column itself.

4. Discussion

As mentioned in Section 3, the evaluation of seabed contributions at the subsurface level and the quantification of the seabed adjacency effects on the upward radiance have been carried out for fixed input parameters in the radiative transfer modeling, namely the phase function of hydrosols and the target radius. In addition, a Lambertian seabed assumption has been considered. In this section, the influence of these parameters and assumption on our results is discussed.

First, the influence of the phase function of the hydrosols on the seabed contributions at the subsurface level is examined. The phase function plays a role in the calculation of the environment function G_{env} [Eq. (8)], which describes the radiative contribution of photons originating from the seabed target to the upward radiance. As illustrated in Fig. 2, the upward radiance is primarily sensitive to the forward scattering peak of the phase function since the target is observed from the sea surface. To investigate the influence of the phase function on the environment function G_{env}, various values of the exponent of the Junge size distribution of the hydrosols (which was set to 4 in Section 3), are selected, namely 3.5, 4 and 4.5. Varying the Junge exponent around the value previously used in Section 3 is relevant because the

magnitude of the forward peak of the phase function is highly sensitive to the size of the hydrosols (i.e., large particles yield a higher forward peak than small particles). Note that the refractive indices of phytoplankton (1.05) and mineral-like particles (1.20) were not changed as compared with Section 3 since the selected values are representative of hydrosols typically found in the ocean. The G_{env} functions obtained for these Junge exponent values are thus compared with the G_{env} function that has been calculated calculated with the Junge exponent set to 4 (Fig. 9).
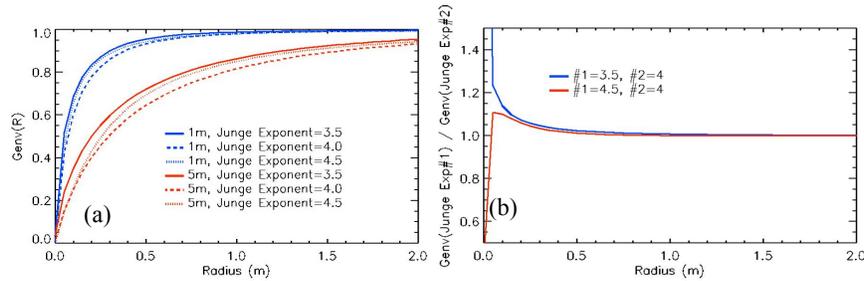

Fig. 9. (a) Variations of the environment function G_{env} with respect to the seabed target radius for different values of the Junge exponent of the size distribution of the hydrosols: 3.5, 4 and 4.5, for H = 1 m and 5 m and for moderately turbid water (same as Fig. 3), (b) ratio of G_{env} calculated for two couples of Junge exponents: (3.5 and 4) and (4.5 and 4) for H = 5 m.

The environment function G_{env} slightly decreases with higher values of the Junge exponent for a given radius [Fig. 9(a)], thus meaning that the influence of the seabed target on the surface radiance is lower for smaller hydrosols. Such a variation is consistent with the fact that the forward peak of the phase function of small hydrosols is less pronounced than that of larger particles (i.e., larger particles contribute more to the diffraction of light). As a result, the contribution of the seabed target is not as efficiently propagated to the water surface as in the case when hydrosols have a larger size. The analysis of the ratios G_{env}(Junge exp. = 3.5)/G_{env}(Junge exp. = 4) and G_{env}(Junge exp. = 4.5)/G_{env}(Junge exp. = 4) [Fig. 9(b)] shows that the sensitivity of G_{env} to the phase function remains lower than 5% when the target size is greater than 0.2 m [Fig. 9(b)], thus demonstrating the weak influence of the phase function on G_{env}. Note that the high values of the ratio observed for a radius lower than 0.2 m are an artifact due to the division by very weak values of G_{env} [Fig. 9(a)].

Second, the impact of the target size on the relative variation of seabed contributions at the subsurface level when accounting for or neglecting seabed heterogeneities (i.e., parameter Δ_{mean}, Eq. (10)) has been examined in the case of moderately turbid water (Table 5).

Table 5. Mean value of the relative variation of seabed contributions Δ_{mean} (in %) as a function of the seabed target radius R for various bottom depth values H (1, 5 and 10 m) and for the moderately turbid water condition. σ is the standard variation (in %).

Target radius R (m)	H = 1 m	H = 5 m	H = 10 m
R = 0.2 m	36 (σ = 25)	102 (σ = 16)	31 (σ = 23)
R = 0.6 m	13 (σ = 12)	57 (σ = 21)	30 (σ = 23)
R = 1 m	6 (σ = 6)	43 (σ = 25)	31 (σ = 23)

For a bathymetry of 5 m, Δ_{mean} regularly decreases from 102% to 57% and 43% when the target radius increases from 0.2 m, 0.6 m to 1 m respectively. Therefore, the seabed contributions could be reduced by a factor of 2 for a target as large as 1 m. Note that the decrease of Δ_{mean} is even more significant (by a factor of 6) in the case of very shallow waters (H = 1 m) as observed in Table 5. These results mean that the influence of seabed heterogeneities on the subsurface radiance is lower for large targets. This is because the photons contributing to the upward radiance mainly originate from the target itself when the latter is large, thus significantly reducing the impact of the neighboring pixels. Note that such a result is consistent with the variation of the environment function G_{env} with the size of the

target, as shown in Fig. 3. It is interesting to note as well that Δ_{mean} is about 30% whatever the target size for deeper waters (H = 10 m). Such a pretty high value of Δ_{mean} means that photons from the seabed still contribute to light at the surface probably because of a higher influence of neighboring pixels. In addition, a careful look on the data showed that the value of the weight $\delta^\uparrow$ (i.e., contribution of the target) remains constant whatever the target size at H = 10 m due to the increased influence of the water column. As a result, the ratio Δ_{mean} is invariant with the target size (based on the definition of Δ, Eq. (10)).

Finally, the influence of the assumption of a Lambertian seabed is examined. It should be highlighted that most of the studies dealing with remote sensing of shallow waters makes the Lambertian assumption for the seabed with a good performance. As an example, the reflectance model developed by Lee et al. [2] is a robust one despite this assumption. However, such an assumption could be discussed due to the potential directional signatures of the material composing the bottom surface, such as sand or aquatic plants. Measurements of the Bidirectional Reflectance Distribution Function (BRDF) of seabed in the ocean (and shallow waters) remain a great challenging task for several reasons. First, it is difficult to operate optical radiometers near the seabed. Second, the protocols for BRDF data acquisition over a given surface are fairly complex to accurately measure the light reflected from the surface at various viewing angles. As a result, there is a lack of available realistic BRDF data that could be introduced in radiative transfer modeling to test the validity of the Lambertian assumption of the seabed. However, Mobley and Sundman [27] showed that the consideration of a BRDF for ocean bottom materials in radiative transfer calculations usually results in errors often much lower than 10% in predicted upwelling radiances as viewed for near-nadir directions (the geometry used for most remote sensing measurements). Doctor et al. [28] have also recently shown that the anisotropy factor normalized to nadir direction is lower than 20% for viewing zenith angles below 50° for a sandy beach surface (see [Fig. 11(c)] in [28]). Note that a sandy beach surface may have similar directional features as a sandy seabed. In addition, they showed that directional effects of a sandy bottom are pronounced in the backscattering plane when the solar zenith angle is lower than 60° and weak in the forward scattering plane, thus suggesting that the impact of seabed BRDF may not be so significant in our configuration of observation. It is here hypothesized that the consideration of seabed BRDF may lead to a weak decrease of the influence of bottom heterogeneities on the subsurface radiance because of the potential loss of photons in the direction of observation (i.e., a higher part of photons coming from the seabed could be scattered out of the field of view). However, such a hypothesis would need to be verified in the future.

5. Summary

In this paper, an original analytical formulation of the subsurface upward radiance based on the radiative transfer theory has been proposed to make explicit the terms representing the contributions of the adjacency effects induced by both heterogeneities in the seabed reflectance and the scattering process within the water column itself. The expression could thus be used either to better understand and quantify the role of the adjacency effects in shallow waters or to develop inverse remote-sensing algorithms for retrieving bottom features such as its composition or its bathymetry. Radiative transfer simulations have been performed for three water turbidity conditions (clear, moderately turbid and turbid waters) using realistic data as inputs such as bottom reflectance spectra that are representative of the Mediterranean Sea.

First, the impact of the sole bottom heterogeneities at the subsurface level has been examined (Section 3.2.1). The results showed that the relative variation of seabed contributions at the subsurface level when accounting for or neglecting seabed heterogeneities [Eq. (10)] is significantly higher (up to a factor of 6 at 450 nm) in the case of a target surrounded by a bright environment (Fig. 5). It has been shown as well that the seabed contributions at the subsurface level could significantly decrease (up to a factor of 6) for

lower bathymetry (from 5 m to 1 m depth), thus meaning that the influence of neighboring pixels is significantly reduced for very shallow waters. Furthermore, a lower influence of the bottom heterogeneity on the subsurface radiance has been observed when the target size increases, as a result of the fact that the photons contributing to the upward radiance mainly originate from the target itself. It has also been shown that the influence of the phase function of hydrosols on these results remains very weak (lower than 5%).

Second, a sensitivity analysis has been carried out to investigate and quantify the impact of all the components of the radiation that contribute to the subsurface upward radiance (i.e., seabed and water column) (Section 3.2.2). Note that this is the first time, to our knowledge, that the contribution of the adjacency effects induced by the seabed and the water column has been quantified for shallow waters. Previous studies dealing with the adjacency effects over coastal waters mostly concerned the influence of the land on the water-leaving radiance measured from satellite sensors [10–12,15]. Our results showed that subsurface measurements of the upward radiation in shallow waters (depth of 5 m) at a high spatial resolution (seabed target size of 0.2 m) could be significantly influenced, by as much as 26%, by the bottom albedo of neighboring pixels when observing a given seabed target. Seabed adjacency effects thus need to be correctly taken into account (or removed) in the processing of remotely-sensed data. Note that the analytical formulation of the subsurface radiance proposed in this study should help to correct for these effects. Note that it was not possible here to rigorously test the validity of the Lambertian assumption of the seabed due to a lack of available realistic BRDF seabed data that could be introduced in radiative transfer modeling. However, on the basis of previous studies (see Section 4), it is believed that the impact of seabed BRDF may not be so significant in our configuration of observation. Such a hypothesis remains to be verified in the future.

The current study is a first step dedicated to understanding the seabed adjacency effects on the subsurface upward radiance. From a closely related perspective, the influence of the multiple scattering processes in the calculation of the environment functions needs to be evaluated. The validity of the Lambertian assumption needs also to be more deeply tested. The influence of the seabed adjacency effects on the above-water radiances (above the sea surface or satellite) should be analyzed as well in further studies as a second step to investigate the remote sensing applications of our results. This is because the implications of our results for the processing of highly resolved remote sensing data such as those measured by drones, satellite sensors, shipborne radiometers or autonomous underwater vehicles are important to improve the quality of the underwater vision. Further work will then consist in using the analytical expression of the subsurface radiance proposed in this study to develop inverse remote sensing algorithms or, at least, to improve their performance, e.g., for mapping the composition of the bottom. Unmixing techniques could be relevant methods for that purpose.

Appendix A: List of notations and abbreviations

BRDF	Bidirectional Reflectance Distribution Function
CDOM	Color Dissolved Organic Matter
OSOAA	Ocean Successive Orders with Atmosphere - Advanced (name of the radiative transfer model [24],)
a_{CDOM}	Absorption coefficient of CDOM (in m^{-1})
$G_{env}(R)$	Contribution of photons originating from a surface of radius R, centered on pixel P, to the upward radiance
H	Bottom depth
E_{tot}	Incident downward flux that reaches the seabed
L_u	Subsurface upward radiance
L_{udp}	Radiance due to photons from the water column which have not previously interacted with the bottom of the ocean
L_B^{dir}	Direct radiance that represents the photons which directly come from a seabed target pixel P up to the sea surface
L_B^{dif}	Radiance that represents the photons from all pixels located in the sea bottom

	(i.e., seabed target P + neighborhood of the target M) and that are scattered towards the direction of observation at the subsurface level (L_B^{dif} is in fact the sum of L_P^{dif} and L_M^{dif})
L_P^{dif}	Diffuse radiance coming from the seabed target P only
L_M^{dif}	Diffuse radiance coming from the environment (i.e., neighboring pixel M) of the seabed target (excluding the target)
M	Neighboring pixel located in the vicinity of the seabed target P
0^-	Subsurface level (i.e., just beneath the air-water interface)
P	Target located at the seabed
$P(\mu)$	Phase function of the hydrosols
PSF	Point Spread Function of water
R	Distance between the center of seabed target pixel P and the center of a neighboring pixel M (i.e., radius of the target) (in m)
CHL	Concentration of chlorophyll a (in mg m^{-3})
SED	Concentration of mineral-like particles (in mg L^{-1})
S_{scene}	Surface of the bottom area that is considered for evaluating the seabed adjacency effects
T_{dir}	Direct upward transmittance of the water column
T_{dif}	Diffuse upward transmittance of the water column
γ_{env}	Environment weight function for the upward radiance
$\delta^{\uparrow}$	Contribution of the reflectance of the seabed target pixel P to the upward radiance
Δ	Relative variation of seabed contributions at the subsurface level when accounting for or neglecting seabed heterogeneities [Eq. (10)]
Δ_{mean}	Mean value of the relative variation Δ calculated over the wavelengths and over the two bottom configurations (cases 1 and 2 in Fig. 4)
ΔAE	Relative difference in the subsurface radiance when accounting for or neglecting seabed heterogeneities $\Delta AE = [L_B^{dif}(\delta)-L_B^{dif}(\delta = 1)]/L_u$. ΔAE actually quantifies the influence of adjacency effects (AE) due to the bottom albedo of neighboring pixels on the upward radiance.
λ	Wavelength (in nm)
μ	Cosine of the scattering angle
ρ_c	Bottom albedo of a bright pixel
ρ_d	Bottom albedo of a dark pixel
$\rho_{env}^{\uparrow}(P)$	Reflectance caused by all the pixels (i.e., the seabed target P and the neighborhood of the target M) located at the sea bottom that contribute to the upward scattered signal
$\rho_n^{\uparrow}(P)$	Reflectance of the neighboring pixels of the seabed target pixel P that contributes to the upward radiance
$\rho_b(M)$	Reflectance of the neighboring pixel M at the sea bottom
ρ_t	Reflectance of the seabed target pixel P at the bottom level
σ	Standard deviation
$\theta_{\downarrow}$	Solar zenith angle beneath the sea surface
$\theta_{\uparrow}$	Zenith viewing angle of the upward radiance in the water
θ_s	Solar zenith angle in the air (in deg)
θ_v	Viewing zenith angle in the air (in deg)
τ_{wtot}	Optical thickness of the oceanic layer

References

1. Z. Lee, K. L. Carder, C. D. Mobley, R. G. Steward, and J. S. Patch, "Hyperspectral remote sensing for shallow waters. I. A semianalytical model," Appl. Opt. **37**(27), 6329–6338 (1998).
2. Z. Lee, K. L. Carder, C. D. Mobley, R. G. Steward, and J. S. Patch, "Hyperspectral remote sensing for shallow waters. 2. Deriving bottom depths and water properties by optimization," Appl. Opt. **38**(18), 3831–3843 (1999).
3. S. Maritorena, A. Morel, and B. Gentili, "Diffuse reflectance of oceanic shallow waters: influence of water depth and bottom albedo," Limnol. Oceanogr. **39**(7), 1689–1703 (1994).
4. V. E. Brando, J. M. Anstee, M. Wettle, A. G. Dekker, S. R. Phinn, and C. Roelfsema, "A physics based retrieval and quality assessment of bathymetry from suboptimal hyperspectral data," Remote Sens. Environ. **113**(4), 755–770 (2009).
5. A. G. Dekker, S. R. Phinn, J. Anstee, P. Bissett, V. E. Brando, B. Casey, P. Fearns, J. Hedley, W. Klonowski, Z. P. Lee, M. Lynch, M. Lyons, C. D. Mobley, and C. Roelfsema, "Intercomparison of shallow water bathymetry, hydro-optics, and benthos mapping techniques in Australian and Caribbean coastal environments," Limnol. Oceanogr. Methods **9**(9), 396–425 (2011).
6. J. Hedley, C. Roelfsema, and S. R. Phinn, "Efficient radiative transfer model inversion for remote sensing applications," Remote Sens. Environ. **113**(11), 2527–2532 (2009).
7. S. Jay and M. Guillaume, "A novel maximum likelihood based method for mapping depth and water quality from hyperspectral remote-sensing data," Remote Sens. Environ. **147**, 121–132 (2014).
8. S. Jay and M. Guillaume, "Regularized estimation of bathymetry and water quality using hyperspectral remote sensing," Int. J. Remote Sens. **37**(2), 263–289 (2016).
9. S. Jay, M. Guillaume, A. Minghelli, Y. Deville, M. Chami, B. Lafrance, and V. Serfaty, "Hyperspectral remote sensing of shallow waters: considering environmental noise and bottom intra-class variability for modeling and inversion of water reflectance," Remote Sens. Environ. **200**, 352–367 (2017).
10. B. Bulgarelli, G. Zibordi, and F. Mélin, "On the minimization of adjacency effects in SeaWiFS primary data products from coastal areas," Opt. Express **26**(18), A709–A728 (2018).
11. B. Bulgarelli and G. Zibordi, "On the detectability of adjacency effects in ocean color remote sensing of mid-latitude coastal environments by SeaWiFS, MODIS-A, MERIS, OLCI, OLI and MSI," Remote Sens. Environ. **209**, 423–438 (2018).
12. B. Bulgarelli, V. Kiselev, and G. Zibordi, "Adjacency effects in satellite radiometric products from coastal waters: a theoretical analysis for the northern Adriatic Sea," Appl. Opt. **56**(4), 854–869 (2017).
13. L. Feng and C. Hu, "Cloud adjacency effects on top-of-atmosphere radiance and ocean color data products: a statistical assessment," Remote Sens. Environ. **174**, 301–313 (2016).
14. V. Kiselev, B. Bulgarelli, and T. Heege, "Sensor independent adjacency correction algorithm for coastal and inland water systems," Remote Sens. Environ. **157**, 85–95 (2015).
15. B. Bulgarelli, V. Kiselev, and G. Zibordi, "Simulation and analysis of adjacency effects in coastal waters: a case study," Appl. Opt. **53**(8), 1523–1545 (2014).
16. S. Belanger, J. K. Ehn, and M. Babin, "Impact of sea ice on the retrieval of water-leaving reflectance, chlorophyll a concentration and inherent optical properties from satellite ocean color data," Remote Sens. Environ. **111**(1), 51–68 (2007).
17. A. Sei, "Analysis of adjacency effects for two Lambertian half-spaces," Int. J. Remote Sens. **28**(8), 1873–1890 (2007).
18. R. Santer and C. Schmechtig, "Adjacency effects on water surfaces: primary scattering approximation and sensitivity study," Appl. Opt. **39**(3), 361–375 (2000).
19. P. N. Reinersman and K. L. Carder, "Monte Carlo simulation of the atmospheric point-spread function with an application to correction for the adjacency effect," Appl. Opt. **34**(21), 4453–4471 (1995).
20. J. Otterman and R. S. Fraser, "Adjacency effects on imaging by surface reflection and atmospheric scattering: cross radiance to zenith," Appl. Opt. **18**(16), 2852–2860 (1979).
21. M. Guillaume, Y. Michels, and S. Jay, *Joint estimation of water column parameters and seabed reflectance combining maximum likelihood and unmixing algorithm*, in 7th Workshop on Hyperspectral Image and Signal Processing: Evolution in Remote Sensing (WHISPERS), (IEEE, 2015, pp.1–4)
22. D. Tanré, M. Herman, P. Y. Deschamps, and A. Leffe, "Atmospheric modeling for space measurements of ground reflectances, including bidirectional properties," Appl. Opt. **18**(21), 3587–3594 (1979).

23. E. Vermote and A. Vermeulen, "Atmospheric correction algorithm: spectral reflectances (MOD09)", NASA MODIS Algorithm Theoretical Basis Document, version 4.0 (1999).

24. M. Chami, B. Lafrance, B. Fougnie, J. Chowdhary, T. Harmel, and F. Waquet, "OSOAA: a vector radiative transfer model of coupled atmosphere-ocean system for a rough sea surface application to the estimates of the directional variations of the water leaving reflectance to better process multi-angular satellite sensors data over the ocean," Opt. Express **23**(21), 27829–27852 (2015), doi:10.1364/OE.23.027829.

25. T. Sagawa, E. Boisnier, T. Komatsu, K. B. Mustapha, A. Hattour, N. Kosaka, and S. Miyazaki, "Using bottom surface reflectance to map coastal marine areas: a new application method for Lyzenga's model," Int. J. Remote Sens. **31**(12), 3051–3064 (2010).

26. J. M. Jaubert, J. R. M. Chisholm, A. Minghelli-Roman, M. Marchioretti, J. H. Morrow, and H. T. Ripley, "Re-evaluation of the extent of Caulerpa taxifolia development in the northern Mediterranean using airborne spectrographic sensing," Mar. Ecol. Prog. Ser. **263**, 75–82 (2003).

27. C. Mobley and L. K. Sundman, "Effects of optically shallow bottoms on upwelling radiances: Inhomogeneous and sloping bottoms," Limnol. Oceanogr. **48**(1), 329–336 (2003).

28. K. Z. Doctor, C. M. Bachmann, D. J. Gray, M. J. Montes, and R. A. Fusina, "Wavelength dependence of the bidirectional reflectance distribution function (BRDF) of beach sands," Appl. Opt. **54**(31), F243–F255 (2015).